Thermal history of the Northern Taiwanese slate belt and implications for wedge growth during the Neogene arc-continent collision

Chih-Tung Chen, Yu-Chang Chan, Olivier Beyssac, Chia-Yu Lu, Yue-Gau Chen, Jacques Malavieille, Steven Kidder, Hao-Cheng Sun

Thermal history of the Northern Taiwanese slate belt and implications for wedge growth during the Neogene arc-continent collision

Chih-Tung Chen[1*], Yu-Chang Chan[2], Olivier Beyssac[3], Chia-Yu Lu[4], Yue-Gau Chen[4], Jacques Malavieille[5], Steven Kidder[6], Hao-Cheng Sun[1]

[1] Department of Earth Sciences, National Central University, Zhongli, Taoyuan, Taiwan, R.O.C.
[2] Institute of Earth Sciences, Academia Sinica, Taipei, Taiwan, R.O.C.
[3] Institut de Minéralogie et de Physique des Milieux Condensés, Université Pierre et Marie Curie, CNRS UMR7590, Paris, France
[4] Department of Geosciences, National Taiwan University, Taipei, Taiwan, R.O.C.
[5] Université de Montpellier, Géosciences Montpellier, Montpellier, France
[6] City College New York, New York City, U.S.A.

*corresponding author, e-mail: chihtung@ncu.edu.tw

Abstract

A significant issue in the study of orogenic systems concerns the roles played by frontal and basal accretion in the construction of orogenic wedges. These different accretion mechanisms result in different thermal histories, with underplated materials experiencing significant heating and deformation during tectonic burial. This work provides new thermal data from Raman spectroscopy of carbonaceous material (RSCM) in combination with structural and stratigraphic observations of the northern Taiwan slate belt to address these questions of wedge development. Sedimentary rocks of the Northern slate belt were deposited on the Chinese continental margin immediately before the onset of the Neogene Taiwan arc-continent collision. In the slates of the northern Hsüehshan Range, a large-scale pop-up structure on the prowedge of the Taiwan Orogen, syn-orogenic metamorphism has been investigated through analyses of peak temperatures and metamorphic field gradients. Results indicate underthrusting of the margin sediments to ~8 km depth with significant folding in two major duplexes occurring before underplating. Such basal accretion is considered responsible for the distinct culmination of the Hsüehshan Range in central Taiwan and its relative uplift with respect to the Backbone Range to the east along the Lishan Fault. A similar underthrusting scenario is also suggested for the Backbone Range Slate Belt. We propose that basal accretion is the predominant mechanism in the growth and evolution of the Taiwan orogenic wedge, and may have been achieved through inversion of a graben system on the ancient passive margin during continental subduction.

1. Introduction

Patterns of metamorphism recorded in mountain belts reflect the underlying tectonic processes driving rock deformation and exhumation (e.g. Huerta et al., 1999; Jamieson et al., 2002; Rosenberg et al., 2015). One important debate related to orogenic belts is the dominant mechanism by which material enters an accretionary wedge. Two endmember scenarios have been proposed: frontal accretion of material at the toe of the wedge (e.g. Barr et al., 1991), or basal accretion by duplexing of underthrust footwall rocks along the main detachment (van Gool and Cawood, 1994; Gutscher et al., 1998; Kukowski et al., 2002). These contrasting wedge formation mechanisms influence a mountain belt's structure as well as its metamorphic and thermal configuration (e.g. Dahlen and Barr, 1989; Bollinger et al., 2004; Simoes and Avouac, 2006; Bonnet et al., 2007; Chen et al., 2011; Konstantinovskaya and Malavieille, 2011; Beyssac et al., 2016; Molli et al., 2018). Terranes composed of frontal-accreted sediments should reveal mainly static diagenesis and retain the thermal signature of the original depositional setting; whereas basal-accreted rocks are expected to exhibit a strong synorogenic (dynamic) metamorphic overprint acquired during the underthrusting stage (Glodny et al., 2005; Konstantinovskaya and Malavieille, 2005). Regional analyses of metamorphic terranes can provide insights into the contribution of these contrasting accretion pathways. Given that it is a type locality for the understanding of wedge mechanics (Davis et al., 1983; Barr et al., 1991), it is important to determine, as best as possible, the accretion mechanisms involved in the active arc-continent collision system of Taiwan.

The Taiwan mountain belt results from oblique convergence between the Eurasian and the Philippine Sea plates. Eastward subduction of the South China Sea beneath the Manila Trench at a rate of ~8 cm per year (Yu et al., 1997; Lin et al., 2010; Fig. 1 inset) led to the oblique collision of the Chinese Continental Margin with the Luzon Arc. This process has been ongoing since the late Miocene (Suppe, 1981, 1984; Teng, 1990). Given its well-constrained and relatively simple tectonic setting, Taiwan offers the opportunity to determine how an extended continental margin covered with a thick pile of sediments (Lin et al., 2003) transforms into an arc-continent collisional prism (e.g. Simoes et al., 2007, 2012; Brown et al., 2012). The Taiwanese orogenic wedge—in which both the basement and cover sediments of the continental margin are bulldozed against the indenting arc—was traditionally considered to have grown by frontal accretion with only minor (<25%) underplating via basal accretion (e.g. Dahlen and Barr, 1989). It follows that thrusts, and associated fault-bend folds (Suppe, 1980; Yue et al., 2005), are directly rooted into a low-dipping detachment fault throughout the orogen (Carena et al., 2002). This inference generally holds true for the outer fold-thrust belt of the orogeny in the Western Foothills. There, the deformed

sedimentary successions display burial diagenesis and an absence of syntectonic prograde metamorphism (Chen and Wang, 1995). However, in the interior part of the mountain belt, orogen-related heating and cooling is recognized in rocks of prehnite-pumpellyite facies up to lower amphibolite facies (e.g. Ernst and Jahn, 1987; Lo and Onstott, 1995; Liu et al., 2001; Fuller et al., 2006; Lee et al., 2006, 2015; Beyssac et al., 2007; Chen et al., 2011, 2018). The distribution of metamorphic grades across the orogen does not exhibit a linear increase from the west (foreland) to the east (hinterland against the backstop) as envisaged in frontal-accreted wedges (Barr et al., 1991). Instead, a high metamorphic temperature anomaly is present in the prowedge Hsüehshan Range (Fig. 1 inset; Beyssac et al., 2007; Simoes et al., 2007, 2012). Further complexity arises from the subducted Chinese continental margin, which possesses numerous Paleogene rifts and grabens related to the opening of the South China Sea (Teng, 1991, 1992; Teng and Lin, 2004). Hence, we find it unlikely that a single, continuous master detachment surface exists beneath the entire orogen. Active shortening on the island as revealed by GPS measurements (Yu et al., 1997; Lin et al., 2010) is localized along the western prowedge and eastern retro-wedge toes rather than being evenly distributed across the entire system as predicted by classical wedge theory (Avouac, 2003; Simoes and Avouac, 2006). Additionally, the vertical displacement field across Taiwan suggests that tectonic underplating is responsible for the spectacular uplift in the Central Range (Simoes et al., 2007; Ching et al., 2011). The above arguments have prompted studies on the nature of accretion in the Taiwan wedge with results advocating substantial tectonic underplating (Fuller et al., 2006; Simoes et al., 2007, 2012; Malavieille, 2010; Chen et al., 2011, 2018; Brown et al., 2012). Other studies, however, have questioned the presence of Neogene prograde metamorphism in the exhumed continental margin basement rocks, as well as the overall significance of underplating (Yamato et al., 2009; Wintsch et al., 2011).

In this study, Raman spectroscopy of carbonaceous material is used as a geothermometer (RSCM; Beyssac et al., 2002; Lahfid et al., 2010) on Paleogene to Miocene continental margin metasediments exhumed in the Taiwanese Central Range slate belt. Unlike the poly-phase metamorphosed continental margin basement now exposed in the Tananao Complex of the eastern Central Range (Fig. 1 inset; Yui et al., 1988, 2009), these rocks are too young to have experienced tectonic events prior to the late Cenozoic arc-continent collision. The highest recorded temperatures of the late Tertiary rocks should therefore reflect either pre-orogenic burial in margin rift basins, or heating during the Neogene orogeny (Beyssac et al., 2007; Chen et al., 2011, 2018). While most past efforts have focused on the central part of the island (e.g. Dahlen and Barr, 1989; Fuller et al., 2006; Simoes et al., 2007), we present new RSCM measurements in the northern part of the slate belt along a NW-trending

transect, the Northern Cross-Island Highway and the Taipingshan Road (Fig. 1). According to the oblique convergence tectonic framework (Suppe, 1981), the northern part of Taiwan has undergone a longer collisional process than further south, and exposes rocks which were once located deeper within the orogenic wedge. Below, we document the history of the northern slate belt using RSCM data on peak thermal conditions together with structural, stratigraphic and published thermal history constraints. This approach allows a quantitative estimate of synorogenic dynamic metamorphism and sheds light on the extent of basal accretion. Structures responsible for underplating are then evaluated, leading to a better understanding of basin inversion atop the subducted continental margin, and a refined tectonic interpretation of the Taiwan arc-continent collision.

2. Regional background

The slate belt of Taiwan outcrops on the prowedge side of the Taiwanese orogenic wedge, and is sandwiched between deformed, un-metamorphosed continental shelf sediments of the Western Foothills and the exhumed continental margin basement of the Tananao Complex. The slate belt comprises two north-south trending zones: the Hsüehshan Range and the Backbone Range Slate Belt (Fig. 1). The Hsüehshan Range contains a continuous succession of Eocene to mid-Miocene continental margin sediments (Teng, 1991) deposited in eastward-deepening rift grabens (Teng, 1992) that were associated with the opening of the South China Sea (Teng and Lin, 2004). The Backbone Range Slate Belt is found east of the Hsüehshan Range and comprised mainly of Miocene pelagic sediments. The Hsüehshan Range and Backbone Range are separated by the Lishan Fault in northern Taiwan. The Backbone Range Slates are juxtaposed to the east against the schist-grade Tananao Complex along a basal unconformity which was reworked as a major shear zone (Suppe et al., 1976; Fisher et al., 2002).

Following the cessation of Mesozoic paleo-Pacific subduction in southeastern China, the continental margin remained subaerial until the early Eocene. Subsequently, grabens developed in the middle part of the margin were drowned, allowing coastal to shallow marine sediments to accumulate (e.g. Lin et al., 2003). During the Oligocene, the grabens deepened and widened in response to the opening of the South China Sea (Briais et al., 1993; Yeh et al., 2010) and thick successions of shelf and distal marine deposits accumulated (Teng, 1992). Following the latest Oligocene, marine sediments draped most of the continental margin. The rifted outer-most rim of the former margin (Lu and Hsu, 1992; Shyu et al., 2005) was covered by minor Eocene deposits and Miocene pelagic shale sequences (Teng, 1991). During the Neogene Taiwan Orogeny some of the rift grabens situated in the distal portions of the continental margin were

inverted as a large-scale pop-up structure forming the Hsüehshan Range (Clark et al., 1993; Tillman and Byrne, 1995; Brown et al., 2012). The Backbone Range Slate Belt is made up of the deformed margin rim cover sediments. Due to the oblique nature of the Taiwanese convergence, the northern parts of the ranges are considered more evolved than their southern counterparts. Exhumed sedimentary successions are not identical along the mountain belt (Teng, 1992) indicating the involvement of different basins along the continental margin.

From bottom to top, the meta-sediments in the northern Hsüehshan Range comprise the following units: Eocene Hsitsun Formation, containing phyllitic slate and intercalated meta-sandstone layers (Fig. 2C); Eocene-Oligocene Szeleng Sandstone, a thick quartzitic arenite to conglomerate; Oligocene Kankou Formation, a massive slate with rare sandstone; Oligocene Tsuku Sandstone, a prominent arenite; interbedded argillites and sandstones of the Oligocene Tatungshan Formation; and uppermost Miocene Sule Formation in which argillite alternates with calcareous sandstones (Fig. 2A and B). The Sule Formation is correlated with lower to middle Miocene sequences found in the un-metamorphosed Western Foothills, suggesting lateral continuation of deposition and facies associations in the Miocene. Occasional volcanics, mostly basaltic, occur intercalated and conformable within the succession. In the eastern part of the northern Hsüehshan Range, Oligocene sediments including the Kankou, Tsuku and Tatungshan formations become indistinguishable as a result of eastward-deepening of the rift basin, and are collectively mapped as the predominantly slate Paling Formation. East of the Lishan Fault, the Backbone Range Slate Belt is composed of massive slate usually assigned as the Miocene Lushan Formation and the Eocene Pilushan Formation. It contains sheared lenses of limestone, sandstone, conglomerates, meta-volcanics and mafic plutonic rocks. The presence of an Eocene ‘formation’ in the Backbone Range Slate Belt remains disputed, as the reported Eocene fossils (Chang, 1972) were from tectonic blocks embedded in the Miocene pelagic mud matrix (Lu and Hsu, 1992).

The sedimentary succession in the northern Hsüehshan Range was thrust over the Western Foothills along the Chuchih Fault and deformed into a series of NE-trending, NW-vergent faults and folds including the Shihtsao Fault, the Loshan Fault, the Chatienshan Anticline, the Tahan Fault, and the Hsitsun Anticline (e.g. Lin and Kuo, 1996; Fig. 1). The Hsüehshan Range is uplifted relative to the Backbone Range along the subvertical E-vergent Lishan Fault which has a complex kinematic history (Lee et al., 1997). Exhumation increases eastward within the Hsüehshan Range as Miocene rocks are found on the flanks of the Chatienshan Anticline and are absent southeast of the Tahan Fault, while Eocene strata crop out only in the core of the Hsitsun Anticline. Degree of metamorphism also increases eastward within the Hsüehshan Range as

slaty cleavage is developed in all rocks southeast of the Junghua Dam on the northwestern limb of the Chatienshan Anticline (the 'onset of cleavage' in Fig. 1) with a NE-trending, inclined to subvertical attitude (Fig. 3A), while the Oligo-Miocene indurate argillite in the exterior Hsüehshan Range possesses only pencil cleavage (Fig. 2). Metamorphic conditions of the Hsüehshan Range span from prehnite-pumpellyite grade to greenschist facies in the Hsitsun anticline (Clark et al., 1993; Chen and Wang, 1995; Beyssac et al., 2007; Chen et al., 2011). Muscovite K-Ar and zircon and apatite fission track ages from the greenschist facies rocks are younger than 5 Ma, indicating cooling during the Taiwanese orogeny (Liu et al., 2001; Fuller et al., 2006; Beyssac et al., 2007).

Based on its thermo-kinematic history, the Hsüehshan Range can be subdivided into upper and lower nappe units (Chen et al., 2011). The current study area in the northern Hsüehshan Range represents the lower nappe unit, in which synorogenic metamorphism is interpreted to overprint earlier lower grade diagenesis (see below). The central and southern Hsüehshan Range belong to the upper nappe unit which is characterized by higher grade, statically-developed diagenetic metamorphism (Beyssac et al., 2007). The cleavage developed in the northern Hsüehshan Range has been constrained from syn-kinematic mica porphyroblasts found in concordant mafic pyroclastic units within the Tatungshan Formation to have been acquired 6 - 2.5 Ma at ~250˚C (Chen et al., 2018).

The Backbone Range Slate Belt is more penetratively deformed, with nappe stacks containing gently-dipping layer-parallel foliation (Fig. 3A) indicating the dominance of top-to-the-northwest shear (Lu and Hsu, 1992; Tillman and Byrne, 1995; Fisher et al., 2002). Overall the Backbone Range Slate Belt to the west of the Tananao Complex consists of a synform or synclinorium (Yang and Lo, 1986). The metamorphic grade in the Backbone Range Slate Belt increases eastward from prehnite-pumpellyite facies at its western border with higher-grade Hsüehshan Range rocks across the Lishan Fault, to biotite grade greenschist facies at its eastern boundary with the schist basement (Ernst and Jahn, 1987; Beyssac et al., 2007). Quantitative assessment of the peak metamorphic conditions, especially the maximum temperature experienced by the rocks of the northern Hsüehshan Range and Backbone Range Slate Belt, is lacking (Chen et al., 2011) and addressed here by applying the RSCM method.

3. Thermometry

3.1. *The Raman spectroscopy of carbonaceous material (RSCM) geothermometer*

Organic matter present in rocks is transformed into graphitic carbonaceous material during metamorphism in a systematic process that can be used as a

geothermometer (e.g. Beyssac et al., 2002, 2019). The graphitization process is irreversible, such that retrograde metamorphic reactions do not affect temperature estimates. The RSCM thermometer is based on the quantification of the degree of ordering of carbonaceous material and has an intrinsic calibration error of ~50 °C due to the petrological data used for calibration. Relative accuracy is better at about 15 °C (Beyssac et al., 2004). For temperatures below 330 °C, Lahfid et al. (2010) performed a systematic study of the evolution of the Raman spectrum of carbonaceous material in low-grade metamorphic rocks in the Glarus Alps (Switzerland). They showed that the Raman spectra of lower temperature carbonaceous material has additional peaks from the spectra observed at higher temperature, and established a quantitative correlation between the degree of ordering of carbonaceous material and temperature. Although this calibration is not universal (see discussion in Lahfid et al., 2010), we use it to obtain first-order insights regarding the thermal evolution of rocks in the study area.

At low temperatures (<330 °C), Raman spectra of carbonaceous material exhibits a graphitic band composed of the G and D2 bands, a defect D composite band made up of the main defect band D1 with the D4 band shoulder, and a small D3 band in between (Lahfid et al. 2010; Beyssac and Lazzeri, 2012). The structural organization of carbonaceous material can be quantified using the R2 and RA1 parameters which reflect the proportion of the D composite band area within the entire measured spectra (R2=D1/[G+D1+D2], RA1=(D1+D4)/[G+D1+D2+D3+D4], where all variables represent band areas). A linear correlation of RA1 with metamorphic temperature is established in the range 210-330°C (Lahfid et al., 2010).

Raman spectra analyses were carried out at Tatung University in Taipei, and ENS, Paris, both using a Renishaw (Wutton-under-Edge, UK) InVIA Reflex microspectrometer equipped with a 514-mm Spectra Physics (20 mW) argon laser. A DMLM Leica (Wetzlar, Germany) microscope with a 50× (100× at ENS) objective (NA=0.90) was utilized to focus the laser on the sample. The laser power at the sample surface was set to be around 1 mW using neutral density filters. The Rayleigh diffusion was eliminated by notch filters, and to attain the optimal spatial resolution the spectrometer entrance slit was closed down to 10 - 15 µm to reach a nearly confocal configuration. The signal was dispersed using an 1800 gr/mm grating and analyzed by a Peltier cooled CCD detector. Calibration of the spectrometer with a silicon standard was carried out before each session. The analytical procedure described in Beyssac et al. (2002, 2003) was adhered to prevent analytical pitfalls. Measurements were done on polished thin sections cut perpendicular to the schistosity, and the carbonaceous material was systematically analyzed below an adjacent transparent mineral, usually quartz. At least ten spectra were recorded for each sample

to smooth out within-sample structural heterogeneity in the extended scanning mode (800 to 2000 cm^{-1}), thereby allowing clear imaging of the entire background signal and proper defining of baseline. The acquired spectra were then processed using the Peakfit software using a five-band solution with Lorentzian band profile, and the parameter RA1 was calculated and utilized to estimate peak temperature (Lahfid et al., 2010). Spectra of the higher temperature sample NCIH-23 were analyzed using a four-band solution following Beyssac et al. (2002), and the peak temperature was inferred through the R2 parameter. As exhibited in Fig. 4 and described in detail below, the carbonaceous material found within metasediments of the northern Taiwan slate belt has a wide range of degree of graphitization similar to that reported in Lahfid et al. (2010).

3.2. *Results from the northern Hsüehshan Range*

A total of 24 samples from the Hsüehshan Range were collected along the Northern Cross-Island Highway and analyzed. Sample spacing was about 1 km in the northwest direction, i.e. perpendicular to the structural grain of the region. The dense sampling was chosen in order to best constrain the thermal history of each strata unit and structure along the transect. Most sampled rocks are massive slates and argillites, along with a few thin slate layers from sandier units (e.g. the Szeleng Sandstone). Representative field and microscopic images are shown in Fig. 2. Sample locations and measurement results are listed in Table 1 and projected on a NW-trending profile in Fig. 3B.

The Raman spectra of carbonaceous material of latest-Oligocene to Miocene indurate argillites and siltite in the outer fringe of the Hsüehshan Range between the Chuchih and Loshan faults (around Fushin and Kaopo villages) are indicative of immature carbonaceous material suggesting peak temperature <200°C (samples NCIH05 to 06-1). These low temperatures are consistent with the argillitic texture of the samples (Fig. 2A and D). Immediately to the southeast of the Loshan Fault, the temperature estimated using the RA1 parameter displays a relatively linear increase from just above 200°C to around 270°C (NCIH07 to 11) at the core of the Chatienshan Anticline (from Miocene Sule Formation down-section to the early Oligocene Kankou Formation). The onset of slaty cleavage development corresponds to an RSCM temperature of 245-265°C (NCIH07-1 and 09). The RSCM temperature drops to 230 - 240°C in the slaty Sule Formation on the southern limb of the Chatienshan Anticline (NCIH12 to 16; Chen et al., 2018) but the rocks still retain slaty cleavage (Fig. 2B and E). The temperature increases again to ~280°C (NCIH17, 18) in the Oligocene Paling Formation in the hanging wall adjacent to the Tahan Fault. The degree of graphitization of carbonaceous material within the slates continues to

rise towards the core of the Hsitsun Anticline. The Oligo-Eocene Szeleng Sandstone at Szeleng has an RSCM temperature of 300 - 310°C (NCIH21, 22 Fig. 2F), and the Eocene Hsitsun Formation at Mingchih reaches 350°C (NCIH23; Fig. 2C). Further southeast the estimated peak temperature is scattered between 260°C to 300°C (NCIH25, 26, 29, and 31). Overall the RSCM temperature increases down-section such that the older and deeper formations of the original sedimentary succession are hotter than overlying units. RSCM temperatures also increase eastward within the Sule Formation (between the limbs of the Chatienshan Anticline), and within the Oligocene strata exposed in the Chatienshan Anticline and hanging wall of the Tahan Fault (the Kankou-Tsuku-Tatungshan series and Paling Formation).

3.3. *Results from the northern Backbone Range Slate Belt*

A total of six samples were collected from within the Backbone Range along the Taipingshan Road. The area is composed predominantly of massive slate which grade to phyllite near Cueifong Lake. A few, sometimes thick, lenses of meta-sandstone are also present. Sample locations and measurement results are listed in Table 1 and projected on the NW-trending profile shown in Fig. 3B.

The RSCM temperature of sample TPS01 is similar to that of samples NCIH29 and 31 on the southeastern end of Northern Cross-Island Highway, implying some structural continuity with the Hsüehshan Range. A significant RSCM temperature drop occurs in the low-hill area near the Lanyang River at Tuchang from ~270°C (TPS01) to ~230°C (TPS02), coinciding with a microstructural change from well-developed slaty cleavage to argillitic texture with incipient slaty cleavage (Fig. 2G and H). Further southeast the estimated peak temperature increases from ~230°C to ~240°C at Jhongjian (TPS04), and ~270°C to ~300°C at Taipingshan and the Cueifong Lake (TPS08, 10 and 13) where phyllitic texture appears (Fig. 2I). The increase of metamorphic temperature towards the southeast with increasing elevation indicates the presence of an inverted metamorphic field gradient also seen in the central Backbone Range (Beyssac et al., 2007) and likely resulting from intense thrust-fold stacking of the Backbone Range slates (Lu and Hsu, 1992).

4. Discussion

4.1. *New quantitative constraints on temperature and comparison with existing data*

The peak temperature estimates using the RSCM method in the northern Hsüehshan Range fit well with patterns exhibited by other geological constraints (Fig. 3B). Zircon fission track ages are completely reset only in the Eocene and lowermost Oligocene rocks along the highway; and, in contrast, younger formations yield partly-reset and unreset ages (Liu et al., 2001). The Hsitsun Formation and Szeleng

Sandstone are thus both the oldest and highest-grade rock units in the region. The trend of rising temperature between the Shihtsao Fault and the Chatienshan Anticline axis is revealed in both the vitrinite reflectance (Chen et al., 2011) and RSCM data sets. The metamorphic temperature assessed from the metamorphic assemblage of a meta-basalt on the northwest limb of the Chatienshan Anticline (Shau and Yang, 1987) is also close to RSCM and vitrinite reflectance-derived temperatures of nearby samples. Illite crystallinity data (Chen et al., 1994) also exhibit a pattern that mirrors the RSCM results: higher temperatures in the cores of the Chatienshan and Hsitsun Anticlines relative to their flanks, and an increase in grade from hanging wall to footwall across the Tahan Fault (Fig. 3B).

Although the thermal history of the sedimentary succession in the northern Hsüehshan Range had already been investigated using illite crystallinity (Chen et al., 1994), zircon fission track dating (Liu et al., 2001), and vitrinite reflectance (Chen et al., 2011), the RSCM data reported here allows a complementary, locally more precise, documentation of peak temperature which conforms well with geological observations. Illite crystallinity data revealed a thermal trend similar to RSCM, but failed to identify the increasing metamorphic temperatures in the Miocene rocks southeast of the Chatienshan Anticline axis. An increase in temperature there is also suggested by the occurrence of penetrative slaty cleavage absent from argillitic counterparts to the northwest that contain only pencil cleavage (Fig. 3B). The vitrinite reflectance (VR) data clearly indicate the greater extent of heating in the Miocene strata southeast of the Chatienshan Anticline than in the exterior portion of the Hsüehshan Range where peak temperatures are 200°C or lower. The diverse peak heating conditions experienced by the rocks east of the Chatienshan Anticline axis was therefore less discriminated in the VR data, and the peak temperatures from VR are exaggerated west of the anticline axis (Fig. 3B). Such discrepancy between VR and RSCM datasets probably arise because the VR calibrations (Barker, 1983; Barker and Goldstein, 1990) applied in Chen et al. (2011) for all the VR data southeast of the cleavage front were poorly constrained, with few constraints for Ro over 3. Consequently, the VR-temperature calibration is saturated in this temperature range (above ~200-250°C) and becomes insensitive. The new RSCM temperatures based on the calibration of Lahfid et al. (2010) provide more realistic and reliable peak temperature estimates that agree with structural observations (Fig. 2). In summary, RSCM thermometry within the meta-sediments appears to sensitively reflect variations of maximum temperature, and is therefore useful for estimating peak burial/metamorphic temperatures in the range ~200°C to ~700°C (Beyssac et al., 2002; Lahfid et al., 2010). When coupled with vitrinite reflectance data for rock units heated under ~200°C, the carbonaceous material geothermometers form valuable tools in

understanding thermal metamorphism across orogens and basins.

4.2. *Extent of synorogenic metamorphic overprint*

The eastward- and down-section-increasing pattern of peak temperature in the Hsüehshan Range may be interpreted as a combination of static (basin burial) and dynamic (orogen-related) metamorphism. This is best illustrated by the thermal evolution of the Miocene strata. At the start of the Miocene, the Chinese continental margin switched from rifting to drifting, which caused shelf-wide thermal subsidence and facilitated a widespread draping of laterally-continuous margin sediments over the more heterogeneous older units (Lin et al., 2003; Teng and Lin, 2004). The Miocene sequence, which lacks abrupt lateral facies changes, can be correlated from the Taiwan Strait all the way through the Coastal Plain, and Western Foothills, to the Hsüehshan Range, then as thinner pelagic shale in Backbone Range Slate Belt (Teng, 1991). Considering the depositional configuration and timing of deposition just prior to the inception of the Neogene arc-continent collision (foreland development at ~6.5 Ma; Lin and Watts, 2002), these c. 2 km thick Miocene strata most likely underwent only minor diagenetic heating prior to structural disruption. For example, even where their stratigraphic equivalents in the Coastal Plain and the Western Foothills were later covered by foreland molasse sediments (Lin and Watts, 2002; Simoes and Avouac, 2006), Miocene sediments were not heated above 100°C (e.g. Chen and Wang, 1995; Kuo, 1997). The ~240°C peak temperature (~200°C temperature increment) recorded by RSCM in the Miocene Sule Formation along the Northern Cross Island Highway is therefore best explained by orogenic loading, since it is equivalent to unmetamorphosed Miocene Mushan to Nankang formations in the Western Foothills (e.g. Teng, 1991). Assuming a geothermal gradient of 25~30°C/km, ~8 km of overburden would be needed to match the observations. This geothermal gradient is consistent with the change of 25-30°C/km in RSCM temperature with stratigraphic depth in the central HR range (Beyssac et al., 2007), the average thermal gradient in exploration wells in Taiwan (Zhou et al., 2003), and it yields reasonable results in thermomechanical models (Simoes et al., 2007) and thermobarometry (e.g. Kidder et al., 2013a).

Depositional patterns of the Eo-Oligocene strata in the Hsüehshan Range indicate isolated eastward-deepening half-grabens with considerable regional variation (Teng and Lin, 2004), much different from their Miocene counterparts. The eastward rise of RSCM temperatures in these rocks may correspond in part to increased basin burial depths (Fig. 3B), thus the relative roles of static and dynamic metamorphism cannot be clearly discerned for these rocks.

Additional salient information regarding the extent of the synorogenic

metamorphic overprint in the northern Hsüehshan Range metasediments is the anomalously low apparent geothermal gradient derived from RSCM data. Along the investigated Northern Cross-Island Highway transect, the sediment succession from the Eocene Hsitsun Formation to the Miocene Sule Formation is estimated to be about 6 km thick (Teng, 1991). The apparent paleothermal field gradient calculated from the RSCM temperatures in the region is below 20°C/km for both the SE limb of the Chatienshan Anticline (based on values of ~270°C in the lower Oligocene Kankou Formation and ~240°C in the Miocene Sule Formation) and from Paling to the core of the Hsitsun Anticline (using values of ~350°C in the Eocene Hsitsun Formation to ~240°C in the Miocene Sule Formation; Fig. 3B). Such values are improbably small for an actively rifting continental margin, since for example, the contemporary geothermal gradient measured and integrated in the Qiongdongnan and Pearl River Mouth basins along the northern border of the South China Sea is mostly above 30°C/km (Yuan et al., 2009). We conclude that the apparent geothermal gradient in northern Hsüehshan Range has thus been reduced by about one-third its original value.

A likely mechanism for the low apparent geothermal gradient is folding that predates peak metamorphism. This results in fold cores with temperatures more similar to temperatures in their limbs than would occur if metamorphism predated folding. We postulate that the presently-exposed continental margin sediment sequence of ~6 km thickness was substantially folded while being underthrust to ~8 km depth where it experienced peak metamorphism, while the vertical distance between the top and bottom of this segment (i.e. Miocene Sule and Eocene Hsitsun formations) had been reduced to ~4 km among the anticline and syncline cores (Fig. 5 A-B) to produce the low, ~20°/km apparent geothermal gradient. A simple model of fold limbs tilted at ~45° prior to peak metamorphism could reduce the apparent geothermal gradient by one-third, i.e. from 30 to 20°/km. Such treatment corresponds with ~33% shortening and ignores the effects of potential vertical thickening and time-dependent aspects of heat diffusion related to the likelihood that folding and metamorphism partly overlapped in time. Assuming that peak metamorphism roughly coincided with peak burial and underplating, a minor amount of folding and shortening followed underplating in order to bring fold limbs to their present geometries (~55° dip, Fig. 5C).

We find it unlikely that post-metamorphic thickening significantly contributed to lowering the apparent geothermal gradient because of the absence of structural or microstructural evidence for this process. For example, there does not appear to be a greater abundance of minor faults or internal penetrative deformation in the North relative to the central Hsüehshan Range, where the apparent geothermal gradient is

similar to the interpreted ancient one (Beyssac et al., 2007). Undetected penetrative thickening is, in any case, less likely in the North due to low temperatures that inhibited deformation mechanisms such as dislocation creep that facilitated penetrative strain in the central Hsüehshan Range (e.g. Kidder et al., 2012). This interpretation of folding prior to metamorphism in the Northern Hsüehshan Range differs from what is interpreted in the central Hsüehshan Range, where a ~30°C/km gradient is preserved, and folding and faulting were interpreted to postdate peak heating (Beyssac et al., 2007).

The RSCM results in the northern Backbone Range Slate Belt along the Taipingshan Road transect are also indicative of dynamic metamorphism overprinting basinal diagenesis. As argued above for the Miocene sediments of the Hsüehshan Range, the Miocene Lushan Formation was incorporated into the Taiwan orogenic pile soon after its deposition, giving little time for diagenetic heating prior to deformation. Peak metamorphic temperatures range from ~230°C in Tuchang/Jhongjian to over 290°C around Cueifong Lake. These temperatures also indicate heating beneath ~8 km of tectonic overburden if a geothermal gradient of ~30°C/km is assumed. The Lushan formation originated as pelagic sediments covering the rifted/drifted Chinese continental margin basement, and sedimentary criteria indicate that the present thickness of the original Lushan sedimentary sequence was likely thinner than the modern 2 km thickness (e.g. Teng, 1992), thus the Lushan sediments are interpreted as including several duplexes. The presence of an inverted metamorphic field gradient in an accretionary setting can also be well explained by a significant component of deformation concurrent with peak metamorphic conditions (e.g. Kidder et al., 2013b).

4.3. *Nappe stacking structure of the Taiwanese slate belt and implications for wedge kinematics*

The new RSCM and structural data reported in the present study, along with existing geothermometric, thermochronological, and structural data of the entire slate belt (e.g. Clark et al., 1993; Liu et al., 2001; Fuller et al., 2006; Beyssac et al., 2007; Brown et al., 2012; Simoes et al. 2012; Chen et al., 2011, 2018) permit a comprehensive evaluation of the geological structures in this part of the orogenic wedge and their potential origin. The Lishan fault—which moved the Hsüehshan Range up relative to the Backbone Range—is poorly exposed in the study area, but its presence is substantiated by an RSCM temperature gap of more than 40°C in the studied transect (Fig. 3B), as well as by structural analyses (Lee et al., 1997; Brown et al., 2012). The enhanced exhumation on the Hsüehshan Range side of the Lishan Fault is consistent with inversion of the Hsüehshan Trough basin controlled by the

geometry of the underlying basement. In this scenario, the basement high east of the Hsüehshan Trough (inherited from Paleogene rifting related to the opening of the South China Sea) pushed the Hsüehshan Range sequences from the east when it subducted beneath the accretionary prism, and evolved into the Tananao Complex now exposed in eastern Central Range. We interpret that the basement-Hsüehshan Range contact developed into a major backthrust, the Lishan Fault, while the Tananao Complex is not yet exposed in the footwall due to being covered by the Lushan Formation (Fig. 6B).

The synorogenic origin of peak metamorphism hypothesized in the previous section strengthens the argument that the northern Hsüehshan Range entered the Taiwan orogenic wedge via basal accretion (as the 'lower nappe' of Chen et al., 2011) rather than frontal accretion. The present peak metamorphic temperature configuration indicates that the lower nappe was underthrust beneath the then accretionary prism (to ~8 km depth) and substantially folded before been incorporated into the orogenic wedge and exhumed. By combining RSCM temperatures, structural data (from km-scale faults and folds, to preliminary microstructural observations), and stratigraphic data, this basal-accreted terrain can be subdivided into two thrust duplexes/nappes (Fig. 6A): the exterior duplex being is the hanging wall of the Shihtsao Fault; the interior one the hanging wall of the Tahan Fault. The exterior duplex consists of relatively younger and more proximal margin sediments (the early Oligocene Kankou Formation to the Miocene Sule Formation) and exhibits generally lower RSCM temperatures (Fig. 3B). This exterior duplex has a simple, uniformly SE-dipping slaty cleavage that likely originated in the inner/proximal portion of the Hsüehshan Trough half-graben system (Teng, 1991). In contrast, the interior duplex is composed of the older and more distal Eo-Oligocene sequence from the Hsitsun Formation to the Paling Formation (the temporal equivalent of the more-proximal Kankou, Tsuku and Tatungshan formations). The interior duplex also has higher RSCM temperatures, and stronger cleavage development and overall deformation. These lower nappe duplexes were basally accreted into the wedge at depths of about 8 km, as determined above based in part on their RSCM temperatures.

The Backbone Range Slate Belt can be characterized as a synclinorium (Yang and Lo, 1986), and nappe stack in which the original sedimentary succession has been multiply folded and transposed, with severely sheared and boudinaged tectonic blocks of various lithologies locally defining broken formations (Lu and Hsu, 1992). Synorogenic prograde heating occurred when these pelagic sediments were underthrust along with the margin basement beneath the accretionary prism. The rapid southeastward rise of peak temperature determined by RSCM, along with the transition from slate to phyllite, indicates the progressive exhumation of more deeply

buried units to the east. These were brought up by reverse faulting and shortening related to the duplexing of the Tananao Complex to the east (the purple unit in Fig. 6B; Fisher et al., 2002; Beyssac et al., 2007; Simoes et al., 2007; Malavieille, 2010; Malavieille et al., 2019), where a second, deeper underplating zone is likely located (Simoes et al., 2007). The rise of RSCM temperature along the Taipingshan Road likely corresponds to cryptic reverse faults which root into the basal thrust (Fig. 6A).

The pre-convergence setting of the Chinese continental margin is illustrated in Fig. 6C, in which the difference between Paleogene (Eo-Oligocene) and Miocene depositional patterns is highlighted. In the initial stage of collision, the rifted continental margin sliver east of the Hsüehshan Trough half-graben (Lu and Hsu, 1992; Shyu et al., 2005) and its overlying Miocene pelagic sediments, were underthrust and buttressed against the leading edge of the Philippine Sea Plate. This caused intense deformation and heating of the Miocene sequence (the present-day Backbone Range slate). This couplet of deformed proto-Tananao Complex and metamorphosed cover sequence then bulldozed the more inboard graben sediments as convergence continued. The deepest and easternmost distal succession within the trough was driven towards the foreland, forming the ‘upper nappe’ unit (Chen et al., 2011) now exposed in south-central Hsüehshan Range. This foreland-ward transport of the statically metamorphosed (Beyssac et al., 2007) ‘upper nappe’ unit was synchronous with tectonic underplating and duplexing of the underthrust proximal Hsüehshan Trough sediments that make up the ‘lower nappe’ units described in this study. The timing of this event was ~6 - 2.5 Ma (Chen et al., 2018), and it culminated with the uplift and exhumation of the present day Hsüehshan Range.

This description implies the presence of multiple active detachment faults in the formation and growth of the Taiwanese accretionary wedge (Malavieille, 2010; Malavieille et al., 2019). The dynamically metamorphosed lower nappe unit is able to crop out in the northern Hsüehshan Range because the northern region has experienced a longer history of uplift and denudation due to oblique and southward-propagating convergence (Suppe, 1981). The upper nappe unit in the north, which presumably resembled the central Hsüehshan Range rocks, has eroded away. Based on the thermokinematic history of the lower nappe unit rocks described above, it is likely that shortening of the Hsüehshan Range rocks likely continues at depth within the orogenic wedge. Such shortening is completed before reaching the surface, since the GPS velocity field (e.g. Yu et al., 1997; Lin et al., 2010) demonstrates that the Hsüehshan Range is extensional at the surface. The Backbone Range slate, however, comprising rift basement cover sediments, continues to be faulted, folded and uplifted together with the thrust stacking and doming of the Tananao Complex (Fisher et al., 2002; Malavieille, 2010; Yui and Chu, 2000).

The temperature-time and structural evolution of the Taiwanese slate depicted above suggests that the Neogene Taiwan arc-continent collision involved significant dynamic heating, particularly by tectonic overloading of underthrusted rocks. Since the cover sediments are found to have experienced prominent synorogenic metamorphism, structurally lower basement rocks are likely to have as well. From this perspective, we find the hypothesis that the Taiwan Orogen experienced little prograde metamorphism, particularly in the Tananao Basement Complex (Yamato et al., 2009; Wintsch et al., 2011), unlikely. In addition to inferences from the metamorphism of overlying sedimentary sequences, heating associated with the Neogene orogeny in the Tananao Basement Complex has been firmly documented in analyses of thermochronologic records (e.g. Lo and Onstott, 1995; Fuller et al., 2006) and is supported by thermal metamorphic modeling (Beyssac et al., 2007; Simoes et al., 2012). Our results also suggest that basins atop highly extended continental margins are able to subduct as a whole to upper-mid crustal depths before being inverted and exhumed. This may have implications for the rheological and tectonic evolution of subducting continents in arc-continent and continent-continent collision zones.

5. Concluding remarks

New RSCM temperature data in northern Taiwan provide evidence of synorogenic metamorphism related to the recent arc-continent collision. Using thermal, structural, and stratigraphic data, we postulate that synorogenic metamorphosed slates in the Hsüehshan Range were underthrust to about 8 km depth and thickened via folding before being basal accreted into the orogenic wedge as two major duplexes. The slates in the northern Backbone Range Slate Belt were tectonically loaded under similar conditions and developed an inverted metamorphic field gradient while being exhumed with the basement Tananao Complex. The inferred deformation was likely accommodated along multiple, possibly simultaneously active, detachment levels. Tectonic underplating is a key mechanism, along with frontal accretion and surface erosion, in the growth, uplift and deformation of the Taiwanese orogenic wedge. Prograde heating is an integral part of the Neogene orogeny and should be considered in kinematic reconstructions.

Acknowledgements

Constructive comments from Guest Editor J. Ali, G. Molli and an anonymous reviewer are deeply appreciated. Support for C.-T. Chen was supplied by MOST grants 106-2119-M-008-023 and 107-2116-M-008-004, S. Kidder was supplied by NSF grant EAR-1524602.

643 References:

644 Avouac, J.P., 2003. Mountain building, erosion, and the seismic cycle in the Nepal
645 Himalaya. Adv. Geophys. 46, 1-80.
646 Barker, C.E., 1983. Influence of time on metamorphism of sedimentary organic matter
647 in liquid-dominated geothermal systems, western North America. Geology 11,
648 384-388.
649 Barker, C.E., Goldstein, R.H., 1990. Fluid-inclusion technique for determining
650 maximum temperature in calcite and its comparison to the vitrinite reflectance
651 geothermometer. Geology 18, 1003-1006.
652 Barr, T.D., Dahlen, F.A., McPhail, D.C., 1991. Brittle frictional mountain building 3:
653 Low-grade metamorphism. J. Geophys. Res. 96-B6, 10319-10338.
654 Beyssac, O., Goffe, B., Chopin, C., Rouzaud, J.N., 2002. Raman spectra of
655 carbonaceous material in metasediments: a new geothermometer. J. Metamorphic
656 Geol. 20, 859-871.
657 Beyssac, O., Brunet, F., Petitet, J.P., Goffe, B., Rouzaud, J.N., 2003. Experimental
658 study of the microtextural and structural transformations of carbonaceous
659 materials under pressure and temperature. Eur. J. Mineral. 15, 937-951.
660 Beyssac, O., Bollinger, L., Avouac, J.-P., Goffe, B., 2004. Thermal metamorphism in
661 the Lesser Himalaya of Nepal determined from Raman spectroscopy of
662 carbonaceous material. Earth Planet. Sci. Lett. 225, 233-241.
663 Beyssac, O., Simoes, M., Avouac, J.-P., Farley, K.A., Chen, Y.-G., Chan, Y.-C., Goffe,
664 B., 2007. Late Cenozoic metamorphic evolution and exhumation of Taiwan.
665 Tectonics 26, TC6001.
666 Beyssac, O., Cox, S.C., Vry, J., Herman, F., 2016. Peak metamorphic temperature and
667 thermal history of the Southern Alps (New Zealand). Tectonophysics 676,
668 229-249.
669 Beyssac, O., Pattison, D.R.M., Bourdelle, F., 2019. Contrasting degrees of
670 recrystallization of carbonaceous material in the Nelson aureole, British Columbia
671 and Ballachulish aureole, Scotland, with implications for thermometry based on
672 Raman spectroscopy of carbonaceous material. Journal of Metamorphic Geology
673 37, 71-95.
674 Bollinger L., Avouac J.P., Beyssac O., Catlos E.J., Harrison T.M., Grove M., Goffe
675 B., and Sapkota S., 2004. Thermal structure and exhumation history of the lesser
676 Himalaya. Tectonics 23, TC5015.
677 Bonnet, C., Malavieille, J., Mosar, J., 2007. Interactions between tectonics, erosion,
678 and sedimentation during the recent evolution of the Alpine orogen: analogue
679 modeling insights. Tectonics 26, TC6016.
680 Briais, A., Patriat, P., Tapponnier, P., 1993. Updated interpretation of magnetic

anomalies and seafloor spreading stages in the South China Sea: Implications for the Tertiary tectonics of Southeast Asia. J. Geophys. Res. 98, 6299-6328.

Brown, D., Alvarez-Marron, J., Schimmel, M., Wu, Y.-M., Camanni, G., 2012. The structure and kinematics of central Taiwan mountain belt derived from geological and seismicity data. Tectonics 31, TC5013.

Buseck, P.R., Betssac, O., 2014. From organic matter to graphite: graphitization. Elements 10, 421-426.

Carena, S., Suppe, J., Kao, H., 2002. Active detachment of Taiwan illuminated by small earthquakes and its control of first-order topography. Geology 30, 935-938.

Chang, L.S., 1972. Eocene/Miocene hiatus and N conglomerate in the Central Range of Taiwan. Proc. Geol. Soc. China 15, 93-98.

Chen, C.-H., Wang, C.-H., 1995. Explanatory notes for the Metamorphic Facies Map of Taiwan, 2nd ed. Special Report of Central Geological Survey 2, 51pp.

Chen, C.-H., Wang, C.-H., Chung, S.-H., 1994. Application of K-mica crystallinity to the study of stratigraphy and structures in the Hsüehshan and Central ranges of Taiwan. Special Publication of the Central Geologic Survey, MOEA, R.O.C. 8, 261-284.

Chen, C.-T., Chan, Y.-C., Lu, C.-Y., Simoes, M., Beyssac, O., 2011. Nappe structure revealed by thermal constraints in the Taiwan metamorphic belt. Terra Nova 23, 85-91.

Chen, C.-T., Chan, Y.-C., Lo, C.-H., Malavieille, J., Lu, C.-Y., Tang, J.-T., Lee, Y.-H., 2018. Basal accretion, a major mechanism for mountain building in Taiwan revealed in rock thermal history. J. Asian Earth Sci. 152, 80-90.

Ching, K.-E., Hsieh, M.-L., Johnson, K.M., Chen, K.-H., Rau, R.-J., Yang, M., 2011. Modern vertical deformation rates and mountain building in Taiwan from precise leveling and continuous GPS observations, 2000-2008. J. Geophys. Res. 116, 08406.

Clark, M.B., Fisher, D.M., Lu, C.-Y., Chen, C.-H., 1993. Kinematic analyses of the Hsueshan Range, Taiwan: a large-scale pop-up structure. Tectonics 12, 205-217.

Dahlen, F.A., Barr, T.D., 1989. Brittle frictional mountain building 1. Deformation and mechanical energy budget. J. Geophys. Res. 94, 3906-3922.

Davis, D., Suppe, J., Dahlen, F.A., 1983. Mechanics of fold-and-thrust belts and accretionary wedges. J. Geophys. Res. 88, 1153-1172.

Ernst, W.G., Jahn, B.M., 1987. Crustal accretion and metamorphism in Taiwan, a post-Palaeozoic mobile belt. Phil. Trans. R. Soc. Lond. A321, 129-161.

Fisher, D.M., Lu, C.-Y., Chu, H.-T., 2002. Taiwan Slate Belt: Insights into the ductile interior of an arc-continent collision, in: Byrne, T.B., Liu, C.-S. (Eds.) Geology and Geophysics of an Arc-Continent Collision, Taiwan. Boulder, Colorado,

719 Geological Society of America Special Paper 358, 93-106.
720 Fuller, C.W., Willett, S.D., Fisher, D., Lu, C.-Y., 2006. A thermomechnical wedge
721 model of Taiwan constrained by fission-track thermochronometry. Tectonophysics
722 425, 1-24.
723 Glodny, J., Lohrmann, J., Echtler, H., Gräfe, K., Seifert, W., Collao, S., Figueroa, O.,
724 2005. Internal dynamics of a paleoaccretionary wedge: insights from combined
725 isotope tectonochronology and sandbox modeling of the South-Central Chilean
726 forearc. Earth Planet. Sci. Lett. 231, 23-39.
727 Gutscher, M.-A., Kukowski, N., Malavieille, J., Lallemand, S., 1998. Episodic
728 imbricate thrusting and underplating: analog experiments and mechanical analysis
729 applied to the Alaskan Accretionary Wedge. J. Geophys. Res. 103, 10161-10176.
730 Huerta, A.D., Royden, L.H., Hodges, K.V., 1999. The effects of accretion, erosion and
731 radiogenic heat on the metamorphic evolution of collisional orogens. J.
732 Metamorphic Geol. 17, 349-366.
733 Jamieson, R.A., Beaumont, C., Nguyen, M.N., Lee, B., 2002. Interaction of
734 metamorphism, deformation and exhumation in large convergent orogens. J.
735 Metamorphic Geol. 20, 9-24.
736 Kidder, S. B., Avouac, J.P., Chan, Y. C., 2012. Constraints from rocks in the Taiwan
737 orogen on crustal stress levels and rheology, Journal of Geophysical Research 117,
738 B09408, doi:10.1029/2012JB009303
739 Kidder, S., Avouac, J.-P., Chan, Y.-C., 2013a. Application of titanium-in-quartz
740 thermobarometry to greenschist facies veins and recrystallized quartzites in the
741 Hsüehshan range, Taiwan. Solid Earth 4, 1-21.
742 Kidder, S.B., Herman, F., Saleeby, J.B., Avouac, J.-P., Ducea, M.N., Chapman, A.D.,
743 2013b. Shear heating not a cause of inverted metamorphism. Geology 41, 899-902,
744 doi:10.1130/ G34289.1
745 Konstantinovskaya, E., Malavieille, J., 2005. Erosion and exhumation in accretionary
746 orogens: Experimental and geological approaches. Geochemistry, Geophysics,
747 Geosystems 6, Q02006.
748 Konstantinovskaya, E., Malavieille, J., 2011. Thrust wedges with decollement levels
749 and syntectonic erosion: A review from analog models. Tectonophysics 502,
750 336-350.
751 Kukowski, N., Lallemand, S.E., Malavieille, J., Gutscher, M.A., Reston, T.J., 2002.
752 Mechanical decoupling and basal duplex for- mation observed in sandbox
753 experiments with application to the Western Mediterranean Ridge accretionary
754 complex. Mar. Geol. 186, 29-42.
755 Kuo, C.-L., 1997. Application of vitrinite reflectance on hydrocarbon exploration in
756 western Taiwan. PhD dissertation, National Taiwan University.

Lafargue, E., Marquis, F. and Pillot, D., 1998. Rock-Eval 6 applications in hydrocarbon exploration, production and soils contamination studies. Oil Gas Sci. Technol., 53, 421–437.

Lahfid, A., Beyssac, O., Deville, E., Negro, F., Chopin, C., Goffe, B., 2010. Evolution of the Raman spectrum of carbonaceous material in low-grade metasediments of the Glarus Alps (Switzerland). Terra Nova 22, 354-360.

Lee, J.-C., Angelier, J., Chu, H.-T., 1997. Polyphase history and kinematics of a complex major fault zone in the northern Taiwan mountain belt: the Lishan Fault. Tectonophysics 274, 97-115.

Lee, Y.-H., Chen, C.-C., Liu, T.-K., Ho, H.-C., Lu, H.-Y., Lo, W., 2006. Mountain building mechanisms in the Southern Central Range of the Taiwan Orogenic Belt - From accretionary wedge deformation to arc-continent collision. Earth Planet. Sci. Lett. 252, 413-422.

Lee, Y.-H., Byrne, T., Wang, W.-H., Lo, W., Rau, R.-J., Lu, H.-Y., 2015. Simultaneous mountain building in the Taiwan orogenic belt. Geology 43, 451-454.

Lin, A.T., Watts, A.B., 2002. Origin of the West Taiwan basin by orogenic loading and flexure of a rifted continental margin. J. Geophys. Res. 107-B9, 2185.

Lin, A.T., Watts, A.B., Hesselbo, S.P., 2003. Cenozoic stratigraphy and subsidence history of the South China Sea margin in the Taiwan region. Basin Res. 15, 453-478.

Lin, K.-C., Hu, J.-C., Ching, K.-E., Angelier, J., Rau, R.-J., Yu, S.-B., Tsai, C.-H., Shin, T.-C., Huang, M.-H., 2010. GPS crustal deformation, strain rate, and seismic activity after the 1999 Chi-Chi earthquake in Taiwan. J. Geophys. Res. 115, B07404.

Lin, M.-L., Kuo, Y.-C., 1996. Degrees of metamorphism in the northern Hsüehshan Range: a study of vitrinite reflectance in metapelites along the Northern Taiwan East-west Cross-Island Highway. J. Geol. Soc. China 39-3, 355-372.

Liu, T.-K., Hsieh, S., Chen, Y.-G., Chen, W.-S., 2001. Thermo-kinematic evolution of the Taiwan oblique-collision mountain belt as revealed by zircon fission track dating. Earth Planet. Sci. Lett. 186, 45-56.

Lo, C.-H., Onstott, T.C., 1995. Rejuvenation of K-Ar systems for minerals in the Taiwan Mountain Belt. Earth Planet. Sci. Lett. 131, 71-98.

Lu, C.-Y., Hsu, K.J., 1992. Tectonic evolution of the Taiwan mountain belt. Petroleum Geol. Taiwan 27, 21-46.

Malavieille, J., 2010. Impact of erosion, sedimentation, and structural heritage on the structure and kinematics of orogenic wedges: Analog models and case studies, GSA Today 20, 4-10.

Malavieille, J., Dominguez, S., Lu, C.-Y., Chen, C.-T., Konstantinovskaya, E., 2019.

795 Deformation partitioning in mountain belts: insights from analogue modeling
796 experiments and the Taiwan collisional orogen. Geological Magazine, doi:
797 10.1017/S0016756819000645.
798 Molli, G., Vitale Brovarone, A., Beyssac, O., Cinquini, I., 2018. RSCM thermometry
799 in the Alpi Apuane (NW Tuscany, Italy): New constraints for the metamorphic and
800 tectonic history of the inner northern Apennines. Journal of Structural Geology
801 113, 200-216.
802 Rosenberg, C.L., Berger, A., Bellahsen, N., Bousquet, R., 2015. Relating orogen
803 width to shortening, erosion, and exhumation during Alpine collision. Tectonics
804 http://dx.doi.org/10.1002/2014TC003736.
805 Shau, Y.-H., Yang, H.-Y., 1987. Petrology of basaltic rocks from Junghua,
806 Taoyuanhsien, northern Taiwan. Proc. Geol. Soc. China 30, 58-82.
807 Shyu, J.B.H., Sieh, K., Chen, Y.-G., 2005. Tandem suturing and disarticulation of the
808 Taiwan orogen revealed by its neotectonic elements. Earth Planet. Sci. Lett. 233,
809 167-177.
810 Simoes, M., Avouac, J. P., 2006, Investigating the kinematics of mountain building in
811 Taiwan from the spatiotemporal evolution of the foreland basin and western
812 foothills., J. Geophys. Res. 111, B10401.
813 Simoes, M., Avouac, J.P., Beyssac, O., Goffe, B., Farley, K.A., Chen, Y.-G., 2007.
814 Mountain building in Taiwan: a thermokinematic model. J. Geophys. Res. 112,
815 B11405.
816 Simoes, M., Beyssac, O., Chen, Y.-G., 2012. Late Cenozoic metamorphism and
817 mountain building in Taiwan: A review, J. Asian Earth Sci. 46, 92-119.
818 Suppe, J., 1980, A retrodeformable cross section of northern Taiwan. Proc. Geol. Soc.
819 China 23, 46-55.
820 Suppe, J., 1981. Mechanics of mountain building and metamorphism in Taiwan.
821 Memoir Geol. Soc. China 4, 67-89.
822 Suppe, J., Wang, Y., Liou, J.G., Ernst, W.G., 1976. Observation of some contacts
823 between basement and Cenozoic cover in the Central Mountains, Taiwan. Proc.
824 Geol. Soc. China 19, 59-70.
825 Teng, L.S., 1990. Geotectonic evolution of late Cenozoic arc-continent collision in
826 Taiwan. Tectonophysics 183, 57-76.
827 Teng. L.S., 1991. Tectonic aspectsof the Paleogene depositional basin of northern
828 Taiwan. Proc. Geol. Soc. China 34, 313-335.
829 Teng, L.S., 1992. Geotectonic evolution of Tertiary continental margin basins of
830 Taiwan. Petroleum Geol. Taiwan 27, 1-19.
831 Teng, L. S., Lin, A. T., 2004. Cenozoic tectonics of the China continental margin:
832 insights from Taiwan, in: Malpas, J., Fletcher, C.J.N., Ali, J., Aitchison, J.C. (Eds.),

Aspects of the Tectonic Evolution of China. Geological Society, London, Special Publications 226, 313-332.

Tillman, K.S., Byrne, T.B., 1995. Kinematic analysis of the Taiwan Slate Belt. Tectonics 14, 322-341.

Van Gool, J.A.M., Cawood, P.A., 1994. Frontal vs. basal accretion and contrasting particle paths in metamorphic thrust belts. Geology 22, 51-54.

Wintsch, R.P., Yang, H.-J., Li, X.-H., Tung, K.-A., 2011. Geochronologic evidence for a cold arc-continent collision: The Taiwan orogeny. Lithos 125, 236-248.

Yamato, P., Mouthereau, F., Burov, E., 2009. Taiwan mountain building: insights from 2-D thermomechanical modeling of a rheologically stratified lithosphere. Geophys. J. Int. 176, 307-326.

Yang, C.-N., Lo, W., 1986. Geologic structures of the Tananao Schist and its cover in the Tayuling area, Central Range of Taiwan. Ti-Chih 7, 11-33.

Yeh, Y.-C., Sibuet, J.-C., Hsu, S.-K., Liu, C.-S., 2010. Tectonic evolution of the Northeastern South China Sea from seismic interpretation. Journal of Geophysical Research 115, B06103.

Yu, S.-B., Chen, H.-Y., Kuo, L.-C., 1997. Velocity field of GPS stations in the Taiwan area. Tectonophysics 274, 41– 59.

Yuan, Y, Zhu, W., Mi, L., Zhang, G., Hu, S., He, L., 2009. “Uniform geothermal gradient” and heat flow in the Qiongdongnan and Pearl River Mouth Basins of the South China Sea. Mar. Petrol. Geol. 26, 1152-1162.

Yue, L.-F., Suppe, J., Hung, J.-H., 2005. Structural geology of a classical thrust belt earthquake: the 1999 Chi-Chi earthquake Taiwan (Mw=7.6). J. Struct. Geol. 27, 2058-2083.

Yui, T.-F., Chu, H.-T., 2000. ‘Overturned’ marble layers: evidence for upward extruion of the Backbone Range of Taiwan. Earth Planet. Sci. Lett. 179, 351-361.

Yui, T.-F., Lu, C.-Y., Lo, C.-H., 1988. A speculative tectonic history of the Tananao Schist of Taiwan. Proc. Geol. Soc. China 31-2, 7-18.

Yui, T.-F., Okamoto, K., Usuki, T., Lan, C.-Y., Chu, H.-T., Liou, J.G., 2009. Late Triassic-late Cretaceous accretion/subduction in the Taiwan region along the eastern margin of South China – evidence from zircon SHRIMP dating. Int. Geol. Rev. 51, 304-328.

Zhou, D., Yu, H.-S., Xu, H.-H., Shi, X.-B., Chou, Y.-W., 2003. Modeling of thermo-rheological structure of lithosphere under the foreland basin and mountain belt of Taiwan. Tectonophysics 374, 115-134, doi:10.1016/s0040-1951(03)00236-1.

Figure captions

Fig. 1: Geologic strip map along the investigated Northern Cross-Island Highway (Hsüehshan Range) and Taipingshan Road (Backbone Range Slate Belt) transect. Inset shows tectonic framework of Taiwan with the slate belt highlighted. Locations of the RSCM samples are marked in yellow and listed in Table 1.

Fig. 2: (A~C) Macroscopic occurrence of outcrops: (A) sand-shale interbedded argillite with only faint pencil cleavage in the Miocene series northwest of cleavage front (site NCIH05-1), width of view ~1 m; (B) meta-siltstone with spaced pressure-solution foliation near NCIH15 in the Miocene series on the southeastern limb of the Chatienshan Anticline; (C) Eocene slate with strong penetrative cleavage at NCIH23. (D~I) Microscopic observation of samples, with 1 mm white scale bars: (D) non-foliated latest Oligocene argillite/siltstone (NCIH07); (E) latest Oligocene argillite/slate with initial cleavage development through pressure solution (NCIH12); (F) Eocene meta-sandstone with sutured quartz grains packed between well-developed cleavage domains (NCIH22, cross-polarized view); (G) Oligocene slate with penetrative slaty cleavage (TPS01); (H) Miocene slate east of the Lishan Fault with patchy pressure solution seams in initial slaty cleavage development (TPS02); (I) Miocene phyllitic slate with dense foliation, growths of quartz porphyroblasts and mica-chlorite aggregates (TPS13).

Fig. 3: (A) Geologic profile of the studied transect along the Northern Cross-Island Highway (NCIH) and Taipingshan Road (TPS) (location marked in Fig. 1), distribution of the RSCM samples (projected), and structural data acquired in this study. (B) Calculated maximum temperature from RSCM measurements of the transect profile, along with published data of vitrinite reflectance (Chen et al., 2011), illite crystallinity (Chen et al., 1994), zircon fission track (Liu et al., 2001) and igneous petrology (Shau and Yang, 1987).

Fig. 4: Raman spectra of CM obtained in the Hsüehshan Range along the Northern Cross-Island Highway (NCIH-06, 07, 09, 17, 20, 21, 23) and the Backbone Range Slate Belt (TPS-02, 04) with the D and G composite bands indicated. The RA1/R2 ratio and corresponding RSCM temperature calculated for each of the depicted spectrum are specified.

Fig. 5: Cartoon of the proposed thermokinematic history of the ‘lower nappe unit’ metasediments between the Shihtsao and Lishan faults along the Northern

Cross-Island Highway in the northern Hsüehshan Range: (I) pre-orogenic setting of the strata in a ~6 km deep basin on the rifted continental margin; (II) peak thermal/metamorphic state when the continental margin was incorporated in the orogenic system and the northern Hsüehshan units were overridden by the accretionary prism, presumably the 'upper nappe unit' now found in the central-southern Hsüehshan Range; (III) retrograde exhumation after basal accretion with continued shortening. Please refer to section 4.2 for details.

Fig. 6: (A) Interpreted structural profile of the northern Taiwan slate belt along the studied road transects. (B) Proposed structural architecture across the northern Taiwan mountain belt. Location is shown in Fig. 1 inset. Detailed duplex structure and thrust stacking of the Hsüehshan and Backbone ranges are enlarged and illustrated in inset. (C) Pre-orogen configuration of the involved sediment successions on the Chinese continental margin (dotted pink denotes margin basement) and the inferred material transport paths of these units (after Teng and Lin, 2004; Simoes et al., 2007; Chen et al., 2011, 2018).

Table

Table 1: RSCM temperature data obtained along the Northern Cross-Island Highway and the Taipingshan Road. Temperatures are calculated following Beyssac et al. (2002) and Lahfid et al. (2010).

Sample	Longitude	Latitude	Altitude,m	Spectra #	RA1/R2 ratio	sdv	T,°C	1σ, °C	se, °C
Northern Cross Island Highway transect									
NCIH05	121.3647	24.7900	389	9	0.50	0.011	<200		
NCIH05-1	121.3580	24.7822	363	7	0.49	0.008	<200		
NCIH06	121.3603	24.7721	487	12	0.52	0.008	<200		
NCIH06-1	121.3474	24.7592	499	11	0.52	0.011	<200		
NCIH07	121.3494	24.7530	510	12	0.55	0.002	211	3	0.87
NCIH07-1	121.3564	24.7504	587	17	0.57	0.004	244	5	1.21
NCIH09	121.3567	24.7286	582	10	0.59	0.004	263	5	1.58
NCIH10	121.3551	24.7151	557	17	0.59	0.004	273	5	1.21
NCIH11	121.3622	24.7088	606	15	0.59	0.003	268	4	1.03
NCIH12*	121.3605	24.6998	632	14	0.57	0.004	246	5	1.34
NCIH13	121.3437	24.6991	654	14	0.56	0.004	225	5	1.34
NCIH15	121.3812	24.6804	563	18	0.56	0.004	236	5	1.18
NCIH16	121.3923	24.6747	676	10	0.57	0.004	247	5	1.58
NCIH17	121.4045	24.6747	685	16	0.60	0.004	277	5	1.25
NCIH18	121.4076	24.6717	730	12	0.60	0.004	283	5	1.44
NCIH19	121.4098	24.6534	903	11	0.59	0.003	271	4	1.21
NCIH20	121.4173	24.6453	919	14	0.61	0.004	292	5	1.34
NCIH21	121.4328	24.6486	1170	15	0.62	0.004	309	5	1.29
NCIH22	121.4418	24.6454	1112	11	0.62	0.003	302	4	1.21
NCIH23	121.4517	24.6404	1121	15	0.65	0.022	351	10	2.58
NCIH25	121.4838	24.6424	1203	13	0.61	0.003	298	4	1.11
NCIH26	121.4818	24.6316	1203	13	0.61	0.004	293	5	1.39
NCIH29	121.4942	24.6057	651	14	0.59	0.002	266	3	0.80
NCIH31	121.5126	24.5980	412	14	0.60	0.003	281	4	1.07
Taipingshan Road transect									
TPS01	121.4945	24.5768	394	17	0.59	0.003	269	4	0.97
TPS02	121.5000	24.5600	504	24	0.56	0.004	227	5	1.02
TPS04	121.5127	24.5458	739	17	0.57	0.004	239	5	1.21
TPS08	121.5242	24.5110	1844	12	0.60	0.004	275	4	1.15
TPS10	121.5372	24.4963	1915	12	0.61	0.004	291	5	1.44
TPS13	121.6075	24.5110	1883	11	0.61	0.004	296	4	1.21

*: data from Chen et al., 2018.

Figure 1.

121°22'
121°26'
121°30'
24°49'
24°47'
24°45'
24°43'
24°41'
24°39'
24°37'
24°35'
24°31'
Fushin
Tt
b
Chuchih Fault
50
Kueishan Fault
Su
Shihtsao Fault
40
25
10
Kaopo
Loshan Fault
Profile
318°
42
85
Onset of cleavage
(Junghua Dam)
Tt
b
Tsk
Kk
Chatienshan Anticline
Northern
Cross-Island
Highway
5
58
Kaoyi
Kk
Tt
Tsk
b
44
Paling
76
85
36
Su
85
86
74
71
82
60
Pl
64
40
82
Szeleng
Tahan Fault
Hsuanyuan Syncline
46
80
68
53
Sl
6
80
Ht
58
34
Mingchih
63
34
70
55
25
47
Sl
68
78
52
42
60
Pl
Hsitsun Anticline
65
Chilan
53
Lanyang River
Valley
Lishan Fault
Tuchang
Lu
Taipingshan
Road
60
Jhongjian
32
42
46
Cueifong Lake
32
30
81
33
37
37
32
40
30
Lu
Taipingshan
N
Legend
Recent alluvial
Lushan Fm (Lu)
Sule Fm (Su)
Tatungshan Fm (Tt)
Tsuku Ss (Tsk)
Kankou Fm (Kk)
Paling Fm (Pl)
Szeleng Ss (Sl)
Hsitsun Fm (Ht)
Mafic volcanics (b)
Syncline
Anticline
Reverse fault
Strike-slip fault
60 Bedding
60 Cleavage
RSCM sample
10 km
120°
121°
122°
25°
24°
23°
22°
N
A
A'
Taipei
Coastal Plain
Western Foothills
Hsuehshan Range
Backbone Range
Slate Belt
Schist Basement Complex
Coastal Range
Ryukyu
subduction
system
82 mm/a
Manila
Trench
100 km

Figure 2.


A


B


C

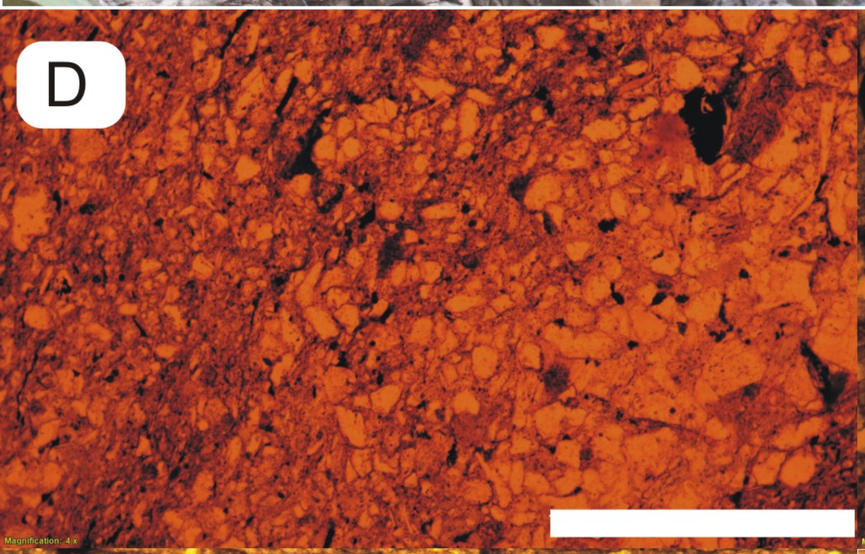
D
Magnification: 4 x

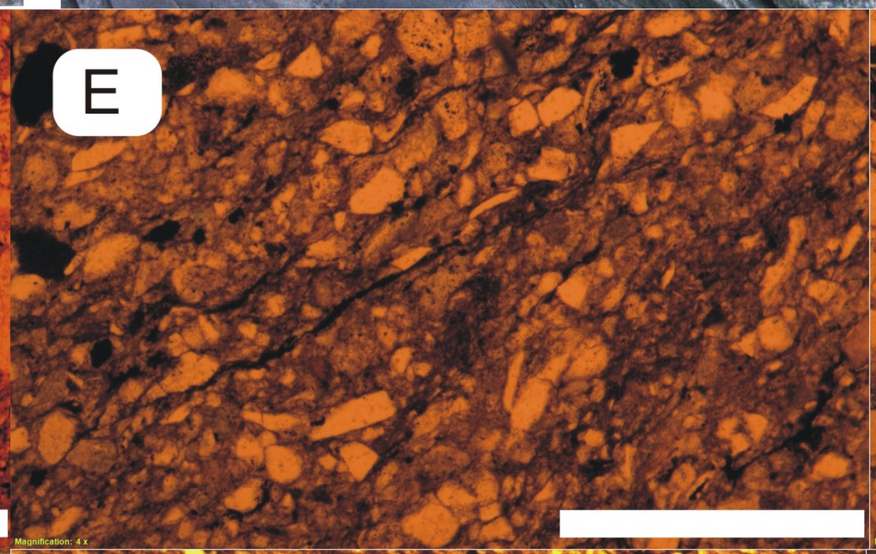
E
Magnification: 4 x

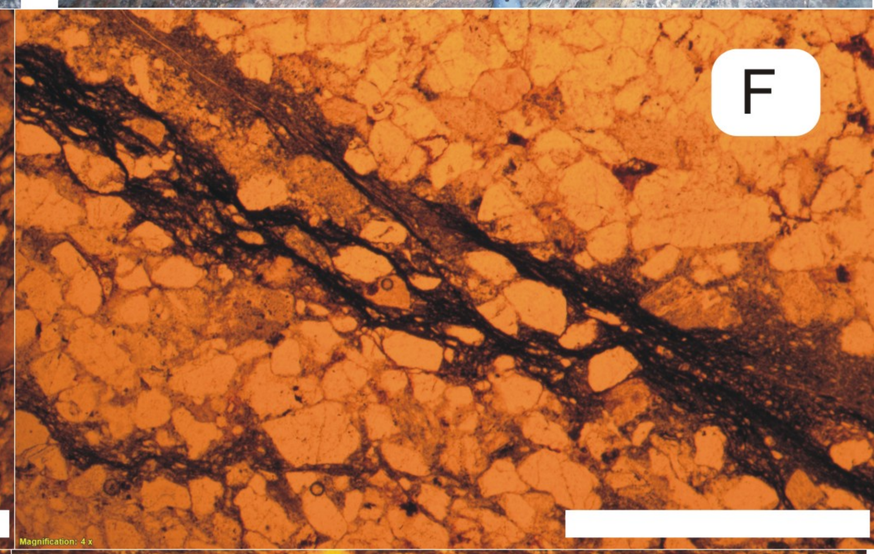
F
Magnification: 4 x

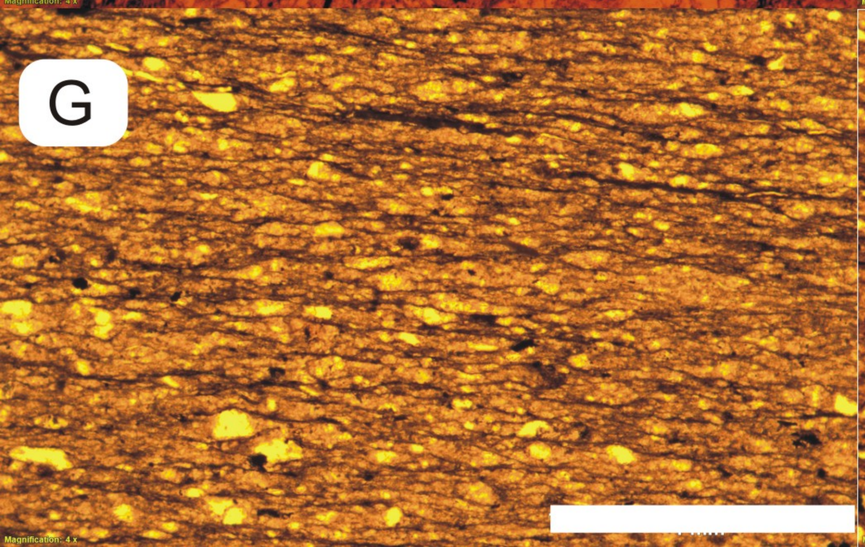
G
Magnification: 4 x

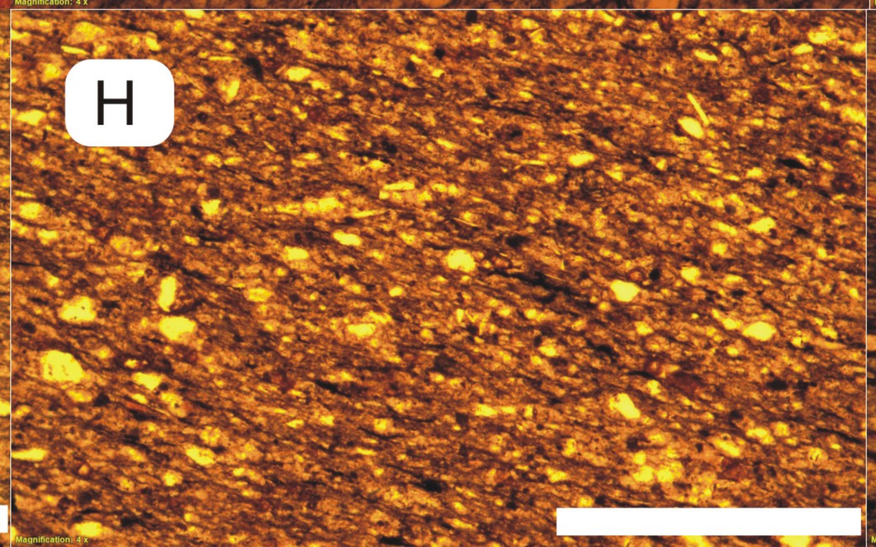
H
Magnification: 4 x

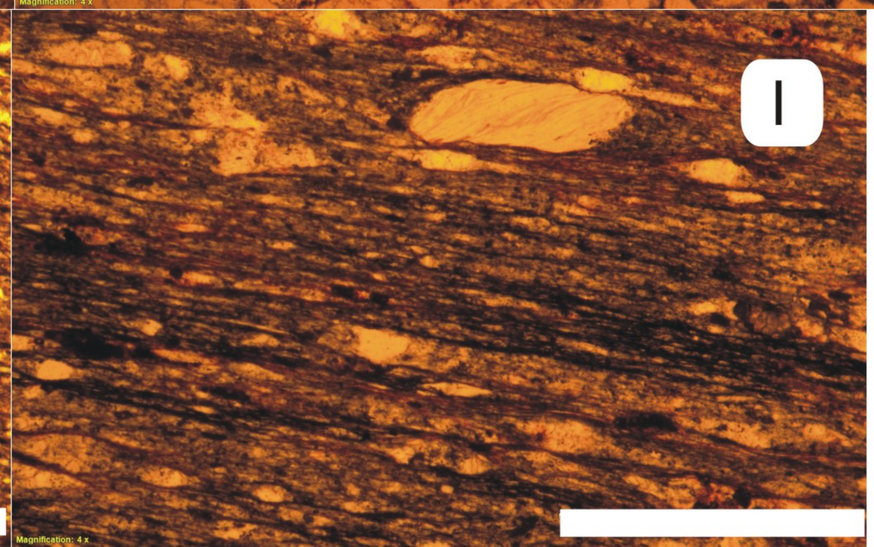
I
Magnification: 4 x

Figure 3.

A

Bedding – Hsuehshan Range

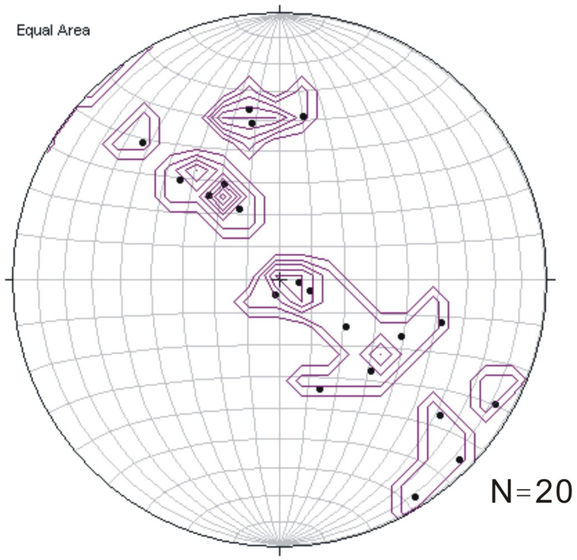

Cleavage – Hsuehshan Range

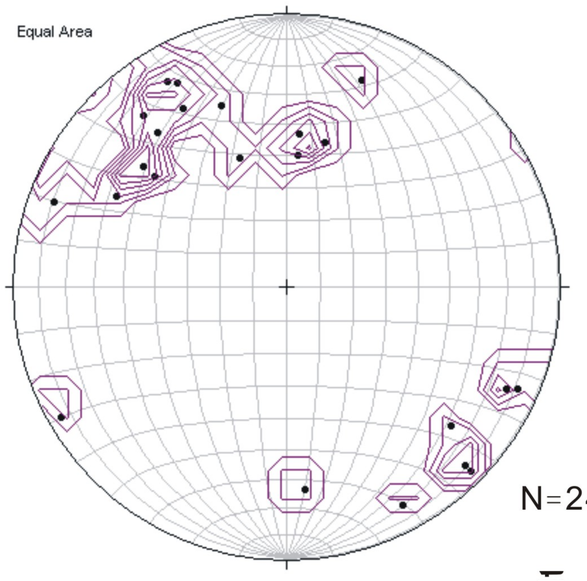

Cleavage – Backbone Range

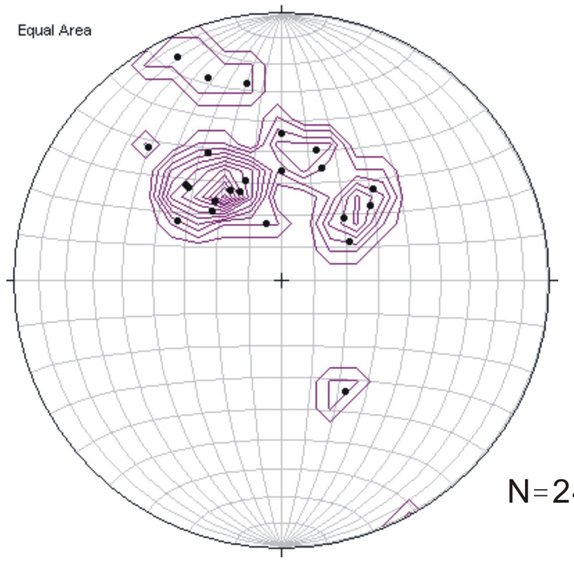

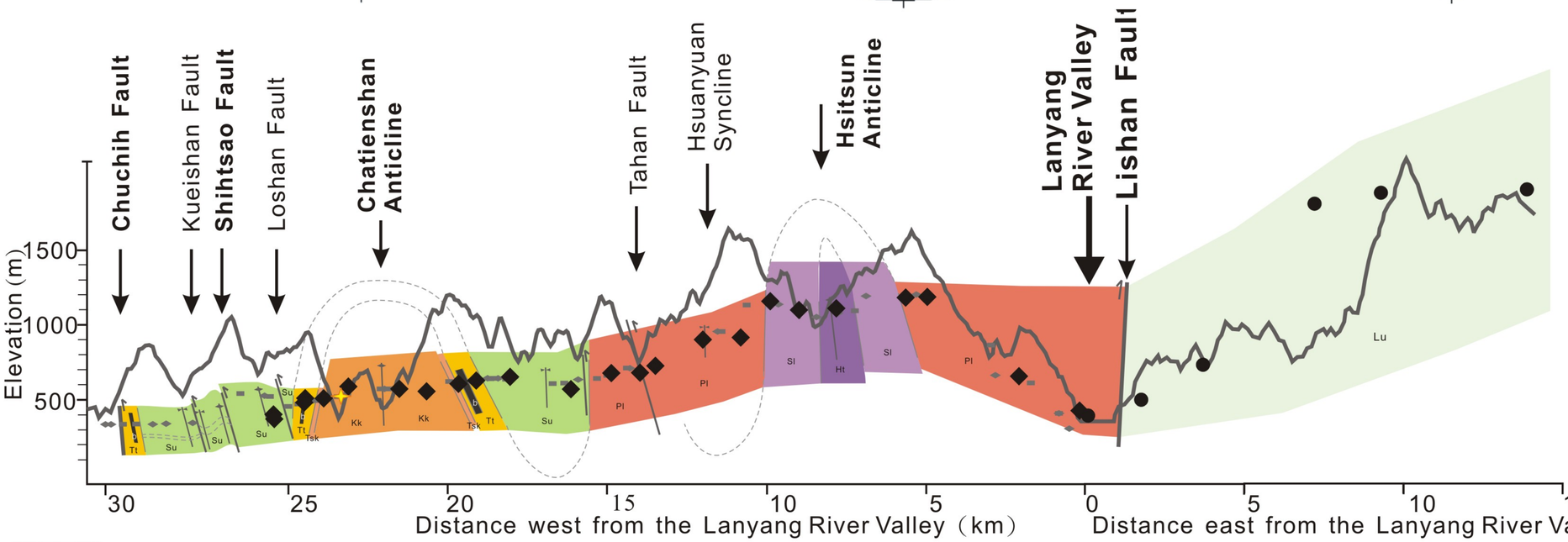

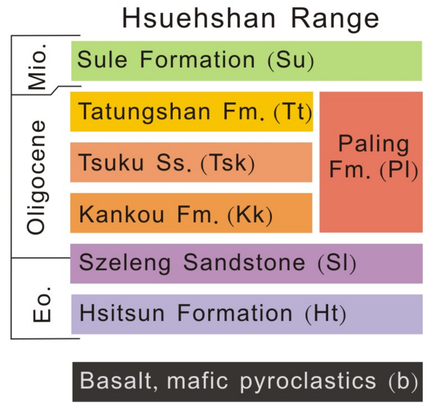

V.E. 5x

B

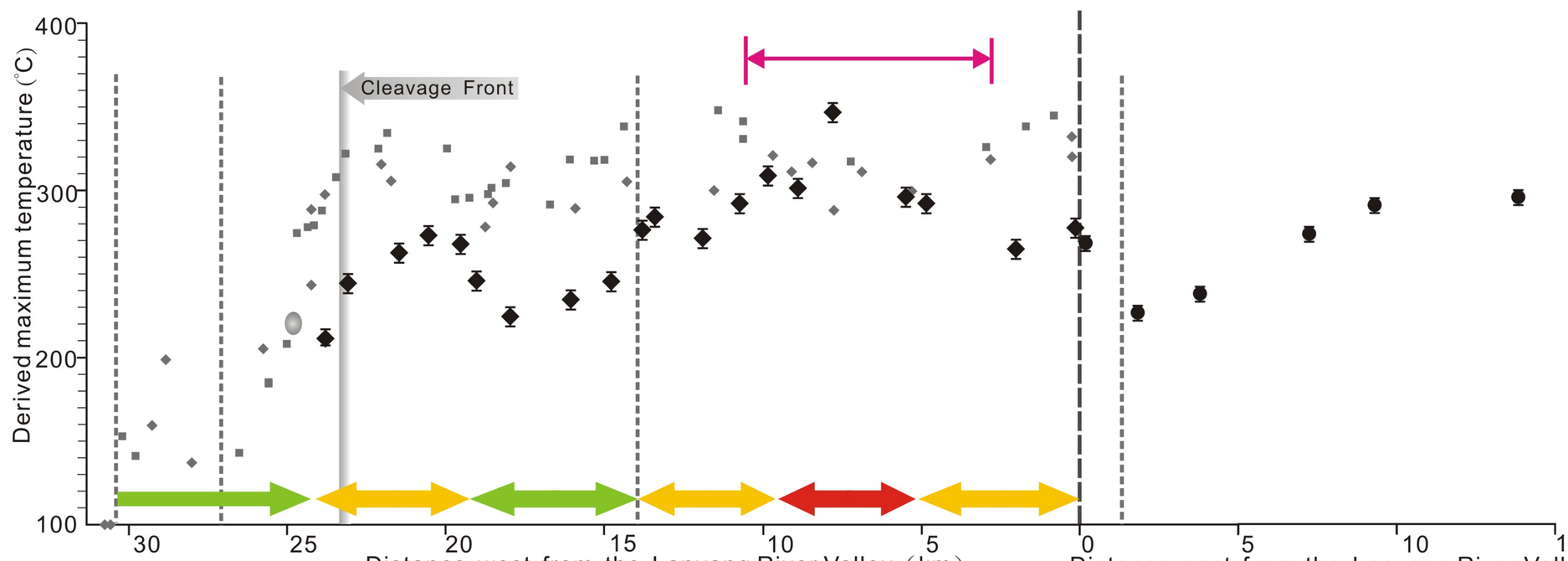

Maximum Temperature derived from Raman spectrum of carbonaceous material measurements (using calibrations of Lahfid et al., 2010 and Beyssac et al., 2002)

- This study- NCIH (Hsuehshan)
- This study- TPS (Backbone)

Maximum Temperature derived from Vitrinite Reflectance measurements (Chen et al., 2011)

- Lin and Kuo, 1996
- Chiu and Chou, 1988

Estimate of metamorphic temperature (assuming pressure at 2 kb) by Shau and Yang (1987)

Zircon fission track complete annealing zone (Liu et al., 2001)

Illite crystallinity (Chen et al., 1994)

Diagenetic zone | Anchizone | Epizone

Figure 4.

D band
G band
NCIH-23
R2=0.65
T=351°C
NCIH-21
RA1=0.62
T=309°C
NCIH-20
RA1=0.61
T=292°C
NCIH-17
RA1=0.60
T=277°C
NCIH-09
RA1=0.59
T=263°C
TPS-04
RA1=0.57
T=239°C
TPS-02
RA1=0.56
T=227°C
NCIH-07
RA1=0.55
T=211°C
NCIH-06
RA1=0.52
T<200°C
Intensity (not to scale)
1000
1500
2000
Raman shift (cm⁻¹)

Figure 5.

(A) Pre-collision setting

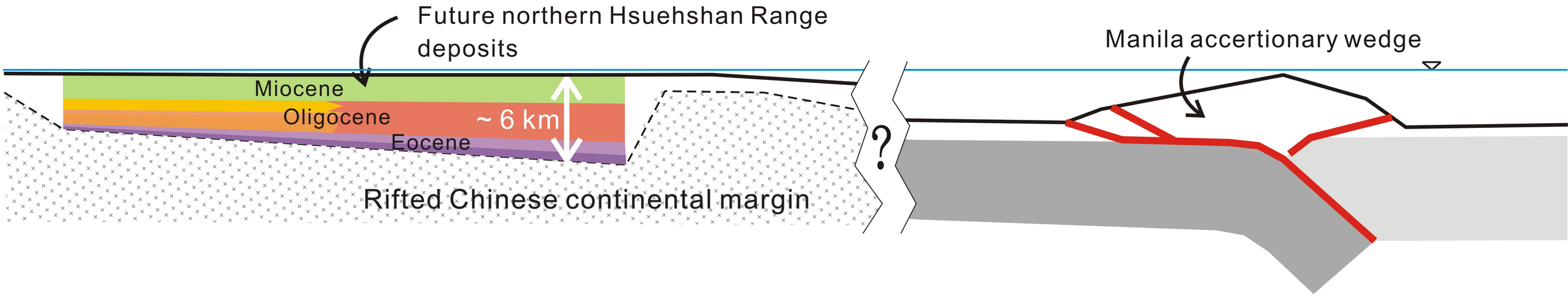

(B) Peak state

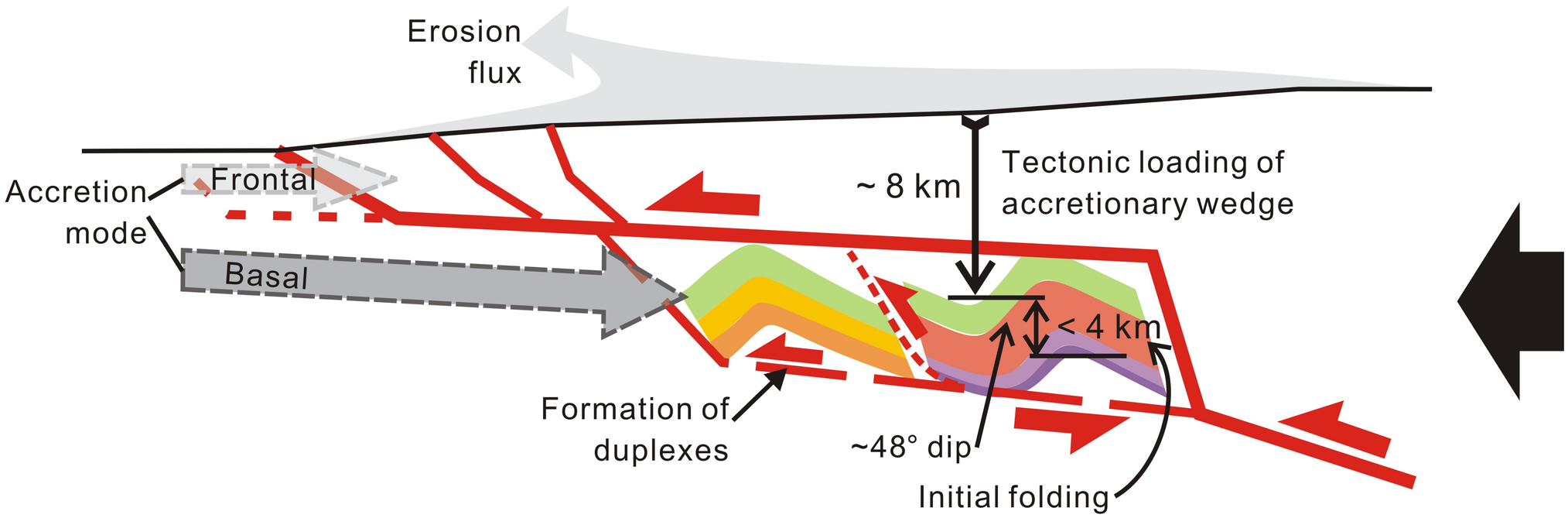

(C) Retrograde exhumation

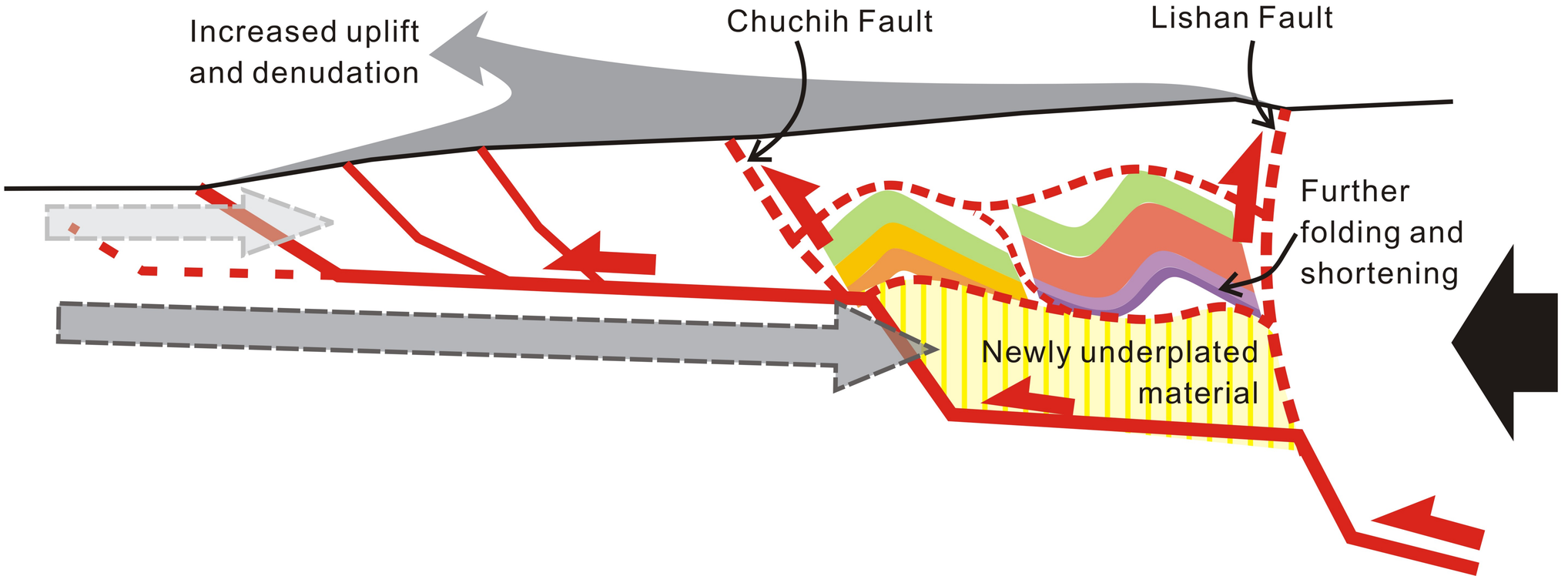

Figure 6.

[A]

Chuchih Fault

Shihtsao Fault

Tahan Fault

Lishan Fault

Stratigraphy

Su

Lu

Tt

Tsk

Kk

Pl

Sl

Ht

Miocene

Oligocene

Oligocene

Eocene

NW

SE

No V.E.

[B]

Western Foothills to Coastal Plain

Hsuehshan Range

Backbone Range

A

A'

Chuchih F.

Lishan F.

frontal thrust

NW

SE

(ceased) subduction

10 km

Western Foothills – Coastal Plain

Foreland sedimentary packages

Hsuehshan Range

eroded

Upper Nappe units

Burial diagenesis dominant

eroded

Lower Nappe units

Significant dynamic metamorphism overprintt

eroded

Shallow duplex units

Backbone Range

eroded

Cover slate series

eroded

Metamorphosed Chinese continental margin basement complex

[C]

The Hsuehshan Trough half-graben

W

E

Miocene

Oligocene

Eocene

?

?

rifted Chinese Continental Margin